Published in final edited form as:
Proteins. 2011 April ; 79(4): 1329–1336. doi:10.1002/prot.22937.

Structural architecture of *Galdieria sulphuraria* DCN1L

E. Sethe Burgie, **Craig A. Bingman**, **Shin-ichi Makino**, **Gary E. Wesenberg**, **Xiaokang Pan**, **Brian G. Fox**, and **George N. Phillips Jr.***
Department of Biochemistry, Center for Eukaryotic Structural Genomics, University of Wisconsin-Madison, Madison Wisconsin 53706-1544

Keywords

Nedd8; Neddylation; *Galdieria sulphuraria*; DCN1; Nedd8 E3 ligase; Cullin-RING E3 ubiquitin ligase; Protein regulation

Introduction

NEDD8ylation is a major regulatory event for cullin-RING E3 ubiquitin ligases (CRL).[1,2] NEDD8ylation activates the ubiquitylation activity of CRLs,[3–5] which serves to regulate a wide variety of cellular processes[6] by selecting specific targets for destruction in the proteasome.[7] NEDD8 E3 ligases catalyze ligation of the ubiquitin-like protein NEDD8 (Rub1 in yeast) to the C-terminal winged-helix domain of the CRL "cullin" subunit.[8] NEDD8ylation increases the ubiquitin (Ub) ligase activity of CRLs by enhancing binding of the CRL RING subunit to Ub-charged Ub-conjugating (E2) enzymes,[9] and by driving conformational changes that permit the RING subunit to productively orient Ub-E2 conjugates with bound CRL substrates for catalysis.[10] However, it is unclear how the NEDD8 E3 ligase catalyses its reaction, what its exact composition is, and how it is regulated. Moreover, current structural and functional models of the NEDD8 E3 ligase are based on the *Saccharomyces cerevisiae* system,[8] in which, an integral NEDD8 E3 ligase subunit, DCN1, has low sequence identity to mammalian DCN1-like proteins, and several amino acid insertions, which together may impede understanding of NEDD8 E3 function in a mammalian system.

Protein NEDD8ylation is analogous to ubiquitylation.[11] NEDD8-activating enzymes (E1), conjugating enzymes (E2), and ligases (E3) are required for the ligation of NEDD8 to its target CRL(s).[2] Each enzyme catalyzes transfer of NEDD8 to its respective acceptor protein through NEDD8's C-terminal glycine carboxylate. First, in an ATP dependent reaction, NEDD8 is covalently linked to the active site cysteine of a heterodimeric E1 enzyme.[12] NEDD8 is then transferred to the active site cysteine of an E2 enzyme (Ubc12).[13] The E3 enzyme complex then serves to ensure reaction specificity and to promote chemical catalysis *en route* to NEDD8 transfer to a specific cullin lysine.[8] The NEDD8 enzyme complex contains the cullin substrate, a RING domain containing subunit with bound NEDD8-E2 conjugate, and a DCN1-like protein (DCN1L).[8]

Mammalian cells utilize five DCN1L paralogs,[14] in contrast to only two cullin-associated RING paralogs.[8] The exact function of each DCN1L is currently unknown. Some DCN1Ls may work in a non-redundant manner as exemplified by human DCN1L3, which preferably

*Correspondence to: Dr. George N. Phillips, Jr., Department of Biochemistry, University of Wisconsin-Madison, 433 Babcock Drive, Madison, WI 53706–1544, Phone: (608) 263–6142, phillips@biochem.wisc.edu.

interacts with human cullin 3 (Cul3), and localizes Cul3 to the plasma membrane.[14] DCN1Ls generally contain two domains, an N-terminal domain that is unique for each paralog, and a conserved C-terminal domain, termed the PONY-domain.[15,16] The purpose of the N-terminal domain is not well understood, but likely aids in reaction specificity and cellular localization.[14] The PONY-domain, however, is integral to protein NEDD8ylation, and is functional in CRL neddylation in the absence of the N-terminal domain.[8,16]

Recently, Scott et al. solved the structure of yeast DCN1 in complex with the winged-helix domain of the *S. cerevisiae* cullin, Cdc53, and provided some clarification for the composition and mechanism of NEDD8 E3s.[8] They identified DCN1 and the *S. cerevisiae* CRL RING subunit, Hrt1, as the major functional components of the yeast NEDD8 E3 ligase. Cdc53 appears to serve as the scaffold for its own NEDD8ylation, as it is already binds Hrt1 in the canonical CRL complex and binds tightly to DCN1.[8] Hrt1 binds the NEDD8-charged E2, Ubc12, and enhances chemical catalysis.[8] DCN1 facilitates catalysis, presumably by optimizing the orientation of the NEDD8-Ubc12 conjugate with the reactive Cdc53 lysine residue.[8]

Here, we report the structure of a DCN1L from *Galdieria sulphuraria* (*Gs*-DCN1L) to 1.3 Å resolution. As all DCN1L structures deposited in the PDB to date are from *S. cereviseae* DCN1 (*Sc*-DCN1), which has low sequence identity and frequent amino acid insertions within its polypeptide chain as compared to mammalian DCN1Ls, we sought a DCN1L that would be more comparable with mammalian forms. *Gs*-DCN1L was identified in genomic sequences[17] and expressed sequence tag data from *G. sulphuraria*.[18] *Gs*-DCN1L was targeted for structural characterization when crystallization trials for the homologous protein, *Mus musculus* Dcn1D1 (*Mm*-Dcn1D1), failed to yield crystals. *Gs*-DCN1L shares higher sequence identity with mammalian DCN1Ls than *Sc*-DCN1, with a low frequency of amino acid insertions and gaps. *Gs*-DCN1L shares 25% amino acid identity with *Sc*-DCN1. At the cullin-binding region *Gs*-DCN1L and *Sc*-DCN1 are very similar in fold and in sequence, indicative of a conserved cullin-binding mode. *Gs*-DCN1L and *Sc*-DCN1 structures diverge markedly near the cullin interaction surface. In this region *Gs*-DCN1L has a disordered loop that exposes a hydrophobic pocket, whereas, the comparable polypeptide segment of *Sc*-DCN1 completely covers the analogous hydrophobic pocket, and is well ordered.[8,15,16] Sequence analysis indicates that this intriguing structural divergence is conserved among *Gs*-DCN1L and the mammalian DCN1L paralogs and may provide clues for additional DCN1L functionalities.

Materials and Methods

Expression and purification

The standard Center for Eukaryotic Structural Genomics (CESG) platform for cloning,[19] protein expression,[20] purification,[21] and bioinformatics management[22] was utilized to produce *Gs*-DCN1L. Briefly, cDNA was cloned into a pEU-His-Flexi vector from cDNA provided by Andreas Weber.[19] Cell-free expression was conducted on a 10-mL scale for 48 hours using WEPRO8240 extract and a Protemist XE protein synthesizer (CellFree Sciences, Yokohama, Japan). Selenomethionine was added to 0.6 mM, and the remaining 19 amino acids were added to 0.3 mM. His-tagged protein was purified by nickel affinity chromatography. The N-terminal His-tag was cleaved with tobacco etch virus protease, and tag-free protein was isolated by subtractive nickel affinity chromatography. Size-exclusion chromatography provided additional purification and permitted exchange of *Gs*-DCN1L into the final protein buffer (5 mM HEPES, 50 mM NaCl, 0.3 mM TCEP, pH 7.0). *Gs*-DCN1L was concentrated to 10 mg/mL, and flash frozen in liquid nitrogen.

Crystallization and structure solution

All crystallization experiments were set up in a sitting drop vapor diffusion format with a TTP Labtech Mosquito (Royston, UK). The UW192 screen (CESG) and the Index HT screen (Hampton Research, Aliso Viejo, California) were utilized to identify crystallization conditions. Crystallization experiments were monitored with and stored in Bruker AXS Crystal Farms (Madison, Wisconsin) operating at 4°C or 20°C. Precipitant solutions for crystal optimization were assembled with a Tecan Genesis RSP 150 (Männedorf, Switzerland).[22]

MAD data were collected from a crystal grown in 27% PEG 1500, 150 mM LiCl, and 100 mM sodium acetate, pH 5.0. Data for structural refinement were collected from a crystal grown in 30% PEG 1500, 150 mM Li_2SO_4, and 100 mM sodium acetate, pH 5.0. The crystals were cryoprotected in fomblin 06/6 and fomblin 18/8, respectively, and flash frozen in a 100 K nitrogen stream. MAD and refinement data were collected at the General Medicine and Cancer Institutes Collaborative Access Team (GM/CA-CAT) 23-ID-D and the Life Sciences Collaborative Access Team (LS-CAT) 21-ID-D beamlines, respectively (Argonne National Laboratory, Argonne, Illinois). Data were indexed, integrated and scaled using HKL2000.[23] Phenix.hyss[24] and ShelXD[25] were employed to evaluate the selenium substructure. Refinement of Se positions, density modification and initial model building were conducted with AutoSharp.[26] Molecular replacement was conducted with Molrep,[27] using the *Gs*-DCN1L model produced by AutoSharp. Successive iterations of model building with Coot[28] and refinement with Phenix.refine[29] yielded the final model. Model validation was conducted with Molprobity[30] and Procheck.[31] Superpositions were conducted with LSQKAB.[32] Structures were presented using PyMOL (DeLano Scientific LLC, San Carlos, California).

Analysis of Gs-DCN1L oligomeric state

Analytical size exclusion gel chromatography was conducted using a 24 ml Superdex 200 GL column (GE Healthcare, Piscataway, New Jersey) with an ÄKTA FPLC chromatographic system (GE Healthcare, Piscataway, New Jersey) at 25°C. 25 μl of sample were loaded per run. Protein elution was monitored by UV absorbance at 280 nm. The elution buffer comprised 200 mM NaCl, 1 mM tris(2-carboxyethyl)phosphine, and 50 mM HEPES, pH 7.5 at 25°C. The column was calibrated with blue dextran, ferritin, conalbumin, carbonic anhydrase, RNase A.

Results and Discussion

Since *Mm*-Dcn1D1 failed to produce crystals in our high-throughput platform, *Gs*-DCN1L was selected as a candidate for structural characterization. *Gs*-DCN1L has higher sequence identity with mammalian DCN1Ls than *Sc*-DCN1, which is the only other structurally characterized DCN1L to date (Figure 1A). Pairwise comparisons of *Gs*-DCN1L and human DCN1L proteins 1–5 (*Hs*-DCN1L) yielded 36–46% amino acid identity over the 199 amino acid *Gs*-DCN1L PONY-domain, while *Sc*-DCN1 and human pairs share 22–26% identity.

Gs-DCN1L was expressed based on gene models from the *G. sulphuraria* genome project.[17,18,33] PONY-domain containing proteins generally comprise two domains, a C-terminal PONY-domain,[16] and a variable N-terminal domain, which may function in regulation, substrate specificity, or cellular localization.[14] Notably, *Gs*-DCN1L lacks an N-terminal domain. Since the PONY-domain of *Sc*-DCN1 is sufficient to stimulate cullin neddylation *in vivo* and *in vitro*,[16] we reasoned *Gs*-DCN1L would provide results of general interest for understanding PONY-domain linked cullin neddylation.

The structure of *Gs*-DCN1L was solved to a resolution of 1.3 Å. MAD phasing of data collected from a single crystal and automated model building yielded an initial model, which was utilized to phase a high-resolution dataset by molecular replacement. The latter dataset was used for structural refinement. Statistics for data collection and structural refinement are provided in Table I. The final *Gs*-DCN1L model contained one selenomethionine, and one oxidized cysteine. Residues 1–3, 165–166, 174–176, and 193–199 were not modeled for lack of interpretable electron density.

The overall fold of *Gs*-DCN1L comprises ten α-helices, and a largely disordered loop made up of residues 164–178 that is located between Helices 9 and 10 (Figure 1B). This loop, which we have termed the "9–10 loop," contains some helical character. The analogous segment of *Sc*-DCN1 (residues 237–254) is well-ordered and contain an additional helix (*Sc*-DCN1 Helix 10). Despite low amino acid sequence identity (25% over 199 amino acid residues), *Gs*-DCN1L and *Sc*-DCN1 superposed with an RMSD of 1.6 Å over 152 matching α-carbons (see Figure 1C). Like *Sc*-DCN1,[15,16] *Gs*-DCN1L contains two EF-hand pairs. The N-terminal EF-hand pair comprises Helices 1–4 and specifically binds Helix 5, while the C-terminal EF-hand pair is composed of Helices 6–9. The solution size of *Gs*-Dcn1L as measured by size exclusion chromatography was 33 kDa. Given that *Gs*-Dcn1L is rod-shaped, and has a molecular weight of 23 kDa, the measured molecular weight is appropriate for *Gs*-DCN1L monomers.

Through structural and functional analyses Scott et al. identified several *Sc*-DCN1 PONY-domain residues that participate in binding of the winged helix domain of the yeast cullin, Cdc53. Matching or analogous *Gs*-DCN1L residues are located in Helices 9 and 10 and in the 9–10 loop (See Figure 1A). This result in addition to conservation of the protein fold (Figure 1C) indicates a conserved cullin-binding mode among DCN1Ls. At the cullin-binding site, *Gs*-DCN1L differs from *Sc*-DCN1, as residues 174–176 are unstructured (Figure 1C). Disorder within this portion of the polypeptide chain may be common among mammalian homologs, as all *Hs*-DCN1Ls except DCN1L3 have a glycine in the position analogous to Gly176 of *Gs*-DCN1L rather than the alanyl residue present in *Sc*-DCN1. *Hs*-DCN1L3 has a glutamate at this position. In this region, *Sc*-DCN1 utilizes the main chain atoms corresponding to *Gs*-DCN1L Asn175 to interact with Cdc53.[8] Consequently, cullin-binding may stabilize this region in *Gs*-DCN1L to resemble *Sc*-DCN1 more closely. Regarding conservation of cullin-binding site residues among the human paralogs, there are some variations (Figure 1A). *Hs*-DCN1L1 and *Hs*-DCN1L2 are practically identical and similar to *Gs*-DCN1L and *Sc*-DCN1. *Hs*-DCN1L4 and *Hs*-DCN1L5 differ at the center of Helix 9, while *Hs*-DCN1L3 varies in the 9–10 loop. Each *Hs*-DCN1L paralog should display subtle differences in their respective cullin-binding surfaces that may provide some reaction specificity, but the overall main chain fold within the cullin-binding face should be quite similar, notwithstanding differences elsewhere within the five N-terminal helices of the PONY-domain.

Since EF-hand pairs generally serve as protein binding modules and the N-terminal EF-hand of the PONY domain binds Helix 5 (Figure 1B and Yang et al.[15]), we employed the Dali search engine[34] to identify analogous EF-hand pairs complexed with an α-helix. Figure 2A shows three cases in which an EF-hand pair binds an α-helix in trans (troponin C-troponin I complex, PDB 1J1E;[35] caltractin-Kar1 complex, PDB 1OQP;[36] Cdc31p-Sfi1p complex, PDB 2GV5[37]). Thus, *Gs*-DCN1L utilizes a common EF-hand conformation to bind Helix 5. This structural feature participates in the juxtaposition of the two EF-hand pairs. The conservation of loop and α-helix length from Helix 1 of the PONY-domain to the loop bridging Helices 5 and 6 is high among DCN1Ls, suggesting that the relative orientation of the two EF-hands has been important in the evolution of DCN1Ls. The importance of the relative positions of the EF-hand pairs has some support as residues of the N-terminal EF-

hand pair influence the ability of *Sc*-DCN1 to facilitate Cdc53 NEDD8ylation through interaction with the N-terminal α-helix of *S. cerevisiae* NEDD8-Ubc12 conjugates.[8] Moreover, alteration in the shape of Ubc12's N-terminal α-helix reduces *Sc*-DCN1's catalytic efficiency. This interaction appears to be important for the proper orientation of the RING-bound NEDD8-Ubc12 conjugate with respect to cullin's reactive lysyl residue.[8] However, it should be noted that human Ubc12 may not form an N-terminal α-helix,[8] and the interactions between NEDD8-Ubc12 and *Hs*-DCN1Ls have not been characterized experimentally.

Enlarged loop size in *Sc*-DCN1, including six additional residues between Helices 7 and 8 (the "7–8 loop,"), and three additional residues within the 9–10 loop (Figure 1A), constitute the most obvious differences in the overalls folds of *Sc*-DCN1 and *Gs*-DCN1L/*Hs*-DCN1Ls. The 7–8 loop differences lead to structural divergence between residues 196–207 of *Sc*-Dcn1 and residues 130–135 of *Gs*-DCN1L. The additional *Sc*-DCN1 residues within the 7–8 loop provides a disparate surface between Helix 5, the C-terminal EF-hand pair adjacent to the 7–8 loop. Effectively, a groove found in this region of *Gs*-DCN1L is absent in *Sc*-DCN1. The structural variations between *Gs*-DCN1L and *Sc*-DCN1 at the 9–10 loop (Helix 10 in *Sc*-DCN1) are points of interest. *Gs*-DCN1L is relatively disordered in this region, while *Sc*-DCN1 is well ordered and has a prominent α-helix (Figure 1C). In *Gs*-DCN1L the 9–10 loop is stabilized by the interaction of Tyr172 with Phe161 of Helix 9 and Trp178, Ile182, Asp183, and Val186 of Helix 10 (Figure 2C). Though these interactions are predominantly hydrophobic in nature, Tyr172 appears to interact with Asp183 via hydrogen bonding. Asp183 maps to Asp259 of the *Sc*-DCN1, which has demonstrable importance in NEDD8ylation in the *S. cerevisiae* system and hydrogen bonds to Lys790 of Cdc53.[8,14,16] Thus, the fact that the highly conserved Tyr172 is the only residue of the 9–10 loop that is noncovalently tethered to the remainder of the PONY domain is likely of functional significance. We hypothesize that Tyr172 is important for the proper positioning of the aspartate with cullin. Ile244 of *Sc*-DCN1 contributes to the stability of the helix corresponding to the *Gs*-DCN1L 9–10 loop, and its interaction with the hydrophobic pocket formed by Helices 8–10 (*Gs*-DCN1L numbering). *Gs*-DCN1L and the *Hs*-DCN1Ls have an aspartate residue in this position (Asp168 in *Gs*-DCN1L, Figure 1A). In *Gs*-DCN1 the corresponding aspartate is solvent exposed and the helical region is rotated away from the comparable position in hydrophobic pocket occupied by Ile244 of *Sc*-DCN1 (Figure 2B). A direct result of the primary sequence differences in the 9–10 loop is that a portion of the hydrophobic cavity formed by Helices 8–10 is solvent exposed in *Gs*-DCN1L. Since the 9–10 loop is highly mobile in this region it is difficult to assess which hydrophobic residues are absolutely exposed. However, the proximity of the hydrophobic pocket to the cullin-binding site is intriguing (Figure 2C), and may serve as a binding site for molecules that would modulate DCN1L function or availability.

Overall, notwithstanding low sequence identity and loop-size differences, the *Gs*-DCN1L fold is similar to *Sc*-DCN1 at the proposed cullin and the NEDD8-E2 conjugate binding regions.[8] This result and the similarity of *Gs*-DCN1L with mammalian DCN1Ls suggest that mammalian DCN1Ls share high secondary and tertiary structural homology at their respective substrate binding sites with both *Gs*-DCN1L and *Sc*-DCN1. Given the relatively high sequence identity of *Gs*-DCN1L for mammalian DCN1Ls, especially types 1 and 2, our structure will provide additional insight to guide experiments designed to probe DCN1L function in mammals. The most glaring difference between *Gs*-DCN1L and *Sc*-DCN1 is the exposed hydrophobic pocket near the 9–10 loop in *Gs*-DCN1L. The sequence similarity among *Gs*-DCN1L and mammalian DCN1Ls in this region suggest that mammalian DCN1Ls will also have an exposed hydrophobic cavity in this region. This striking feature of *Gs*-DCN1L suggests that some DCN1Ls may bind additional molecules, which could modulate their function.

Acknowledgments

This work was supported by the NIH Protein Structure Initiative Grant GM074901. We gratefully acknowledge all members of the Center for Eukaryotic Structural Genomics. We would like to thank Chris Bianchetti and Aram Chang for reviewing the manuscript. We thank Dr. Andreas Weber for providing cDNA and pre-publication releases of the *Galdieria sulphuraria* genomic and EST sequences. We thank LS-CAT Sector 21 for use of their facilities in the collection of the final high-resolution dataset. Use of LS-CAT Sector 21 was supported by the Michigan Economic Development Corporation and the Michigan Technology Tri-Corridor (Grant 085P1000817). We thank the GM/CA CAT staff for facilitating collection of the phasing data sets. GM/CA CAT has been funded in whole or in part with Federal funds from the National Cancer Institute (Y1-CO-1020) and the National Institute of General Medical Science (Y1-GM-1104). Use of the Advanced Photon Source was supported by the U.S. Department of Energy, Basic Energy Sciences, Office of Science, under contract No. DE-AC02-06CH11357.

References

1. Lammer D, Mathias N, Laplaza JM, Jiang WD, Liu Y, Callis J, Goebl M, Estelle M. Modification of yeast Cdc53p by the ubiquitin-related protein Rub1p affects function of the SCFCdc4 complex. Gene Dev. 1998; 12(7):914–926. [PubMed: 9531531]
2. Merlet J, Burger J, Gomes JE, Pintard L. Regulation of cullin-RING E3 ubiquitin-ligases by neddylation and dimerization. Cell Mol Life Sci. 2009; 66(11–12):1924–1938. [PubMed: 19194658]
3. Morimoto M, Nishida T, Honda R, Yasuda H. Modification of cullin-1 by ubiquitin-like protein Nedd8 enhances the activity of SCFskp2 toward p27(kip1). Biochem Bioph Res Co. 2000; 270(3): 1093–1096.
4. Podust VN, Brownell JE, Gladysheva TB, Luo RS, Wang CH, Coggins MB, Pierce JW, Lightcap ES, Chau V. A Nedd8 conjugation pathway is essential for proteolytic targeting of p27(Kip1) by ubiquitination. P Natl Acad Sci USA. 2000; 97(9):4579–4584.
5. Read MA, Brownell JE, Gladysheva TB, Hottelet M, Parent LA, Coggins MB, Pierce JW, Podust VN, Luo RS, Chau V, Palombella VJ. Nedd8 modification of Cul-1 activates SCF beta(TrCp)-dependent ubiquitination of I kappa B alpha. Molecular and Cellular Biology. 2000; 20(7):2326–2333. [PubMed: 10713156]
6. Deshaies RJ. SCF and cullin/RING H2-based ubiquitin ligases. Annu Rev Cell Dev Bi. 1999; 15:435–467.
7. Ciechanover A. The Ubiquitin-Proteasome Proteolytic Pathway. Cell. 1994; 79(1):13–21. [PubMed: 7923371]
8. Scott DC, Monda JK, Grace CR, Duda DM, Kriwacki RW, Kurz T, Schulman BA. A dual E3 mechanism for Rub1 ligation to Cdc53. Mol Cell. 2010; 39(5):784–796. [PubMed: 20832729]
9. Kawakami T, Chiba T, Suzuki T, Iwai K, Yamanaka K, Minato N, Suzuki H, Shimbara N, Hidaka Y, Osaka F, Omata M, Tanaka K. NEDD8 recruits E2-ubiquitin to SCF E3 ligase. Embo Journal. 2001; 20(15):4003–4012. [PubMed: 11483504]
10. Duda DM, Borg LA, Scott DC, Hunt HW, Hammel M, Schulman BA. Structural insights into NEDD8 activation of Cullin-RING ligases: Conformational control of conjugation. Cell. 2008; 134(6):995–1006. [PubMed: 18805092]
11. Tanaka K, Suzuki T, Chiba T. The ligation systems for ubiquitin and ubiquitin-like proteins. Mol Cells. 1998; 8(5):503–512. [PubMed: 9856335]
12. Huang DT, Schulman BA. Expression, purification, and characterization of the E1 for human NEDD8, the heterodimeric APPBP1-UBA3 complex. Ubiquitin and Protein Degradation, Part A. 2005; 398:9–20.
13. Chiba T. In vitro systems for NEDD8 conjugation by Ubc12. Ubiquitin and Protein Degradation, Part A. 2005; 398:68–73.
14. Meyer-Schaller N, Chou YC, Sumara I, Martin DD, Kurz T, Katheder N, Hofmann K, Berthiaume LG, Sicheri F, Peter M. The human Dcn1-like protein DCNL3 promotes Cul3 neddylation at membranes. Proc Natl Acad Sci U S A. 2009; 106(30):12365–12370. [PubMed: 19617556]
15. Yang XY, Zhou J, Sun L, Wei ZY, Gao JY, Gong WM, Xu RM, Rao ZH, Liu YF. Structural basis for the function of DCN-1 in protein neddylation. Journal of Biological Chemistry. 2007; 282(34): 24490–24494. [PubMed: 17597076]

16. Kurz T, Chou YC, Willems AR, Meyer-Schaller N, Hecht ML, Tyers M, Peter M, Sicheri F. Dcn1 functions as a scaffold-type E3 ligase for cullin neddylation. Mol Cell. 2008; 29(1):23–35. [PubMed: 18206966]

17. Barbier G, Oesterhelt C, Larson MD, Halgren RG, Wilkerson C, Garavito RM, Benning C, Weber APM. Comparative genomics of two closely related unicellular thermo-acidophilic red algae, Galdieria sulphuraria and Cyanidioschyzon merolae, reveals the molecular basis of the metabolic flexibility of Galdieria sulphuraria and significant differences in carbohydrate metabolism of both algae. Plant Physiol. 2005; 137(2):460–474. [PubMed: 15710685]

18. Weber APM, Oesterhelt C, Gross W, Brautigam A, Imboden LA, Krassovskaya I, Linka N, Truchina J, Schneidereit J, Voll H, Voll LM, Zimmermann M, Jamai A, Riekhof WR, Yu B, Garavito RM, Benning C. EST-analysis of the thermo-acidophilic red microalga Galdieria sulphuraria reveals potential for lipid A biosynthesis and unveils the pathway of carbon export from rhodoplasts. Plant Mol Biol. 2004; 55(1):17–32. [PubMed: 15604662]

19. Blommel PG, Martin PA, Wrobel RL, Steffen E, Fox BG. High efficiency single step production of expression plasmids from cDNA clones using the Flexi Vector cloning system. Protein Expr Purif. 2006; 47(2):562–570. [PubMed: 16377204]

20. Makino S, Goren MA, Fox BG, Markley JL. Cell-free protein synthesis technology in NMR high-throughput structure determination. Methods Mol Biol. 2010; 607:127–147. [PubMed: 20204854]

21. Vinarov DA, Newman CL, Tyler EM, Markley JL, Shahan MN. Wheat germ cell-free expression system for protein production. Curr Protoc Protein Sci. 2006; Chapter 5(Unit 5):18. [PubMed: 18429309]

22. Zolnai Z, Lee PT, Li J, Chapman MR, Newman CS, Phillips GN Jr, Rayment I, Ulrich EL, Volkman BF, Markley JL. Project management system for structural and functional proteomics: Sesame. J Struct Funct Genomics. 2003; 4(1):11–23. [PubMed: 12943363]

23. Otwinowski Z, Minor W. Processing of X-ray diffraction data collected in oscillation mode. Method Enzymol. 1997; 276:307–326.

24. Grosse-Kunstleve RW, Adams PD. Substructure search procedures for macromolecular structures. Acta Crystallogr D Biol Crystallogr. 2003; 59(Pt 11):1966–1973. [PubMed: 14573951]

25. Schneider TR, Sheldrick GM. Substructure solution with SHELXD. Acta Crystallogr D Biol Crystallogr. 2002; 58(Pt 10 Pt 2):1772–1779. [PubMed: 12351820]

26. Vonrhein C, Blanc E, Roversi P, Bricogne G. Automated structure solution with autoSHARP. Methods Mol Biol. 2007; 364:215–230. [PubMed: 17172768]

27. Vagin A, Teplyakov A. MOLREP: an automated program for molecular replacement. Journal of Applied Crystallography. 1997; 30:1022–1025.

28. Emsley P, Cowtan K. Coot: model-building tools for molecular graphics. Acta Crystallogr D Biol Crystallogr. 2004; 60(Pt 12 Pt 1):2126–2132. [PubMed: 15572765]

29. Afonine PV, Grosse-Kunsteve RW, Adams PD. The Phenix refinement framework. CCP4 Newsl. 2005; 42 contribution 8.

30. Davis IW, Leaver-Fay A, Chen VB, Block JN, Kapral GJ, Wang X, Murray LW, Arendall WB 3rd, Snoeyink J, Richardson JS, Richardson DC. MolProbity: all-atom contacts and structure validation for proteins and nucleic acids. Nucleic Acids Res. 2007; 35(Web Server issue):W375–383. [PubMed: 17452350]

31. Laskowski RA, Macarthur MW, Moss DS, Thornton JM. Procheck - a Program to Check the Stereochemical Quality of Protein Structures. Journal of Applied Crystallography. 1993; 26:283–291.

32. Kabsch W. Solution for Best Rotation to Relate 2 Sets of Vectors. Acta Crystallographica Section A. 1976 Sep; 32(1):922–923.

33. Michigan State University Galdieria Database. http://genomics.msu.edu/galdieria

34. Holm L, Kaariainen S, Rosenstrom P, Schenkel A. Searching protein structure databases with DaliLite v. 3. Bioinformatics. 2008; 24(23):2780–2781. [PubMed: 18818215]

35. Takeda S, Yamashita A, Maeda K, Maeda Y. Structure of the core domain of human cardiac troponin in the Ca(2+)-saturated form. Nature. 2003; 424(6944):35–41. [PubMed: 12840750]

36. Hu H, Chazin WJ. Unique features in the C-terminal domain provide caltractin with target specificity. J Mol Biol. 2003; 330(3):473–484. [PubMed: 12842464]

37. Li S, Sandercock AM, Conduit P, Robinson CV, Williams RL, Kilmartin JV. Structural role of Sfi1p-centrin filaments in budding yeast spindle pole body duplication. J Cell Biol. 2006; 173(6): 867–877. [PubMed: 16785321]

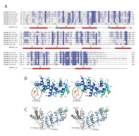

Figure 1. Sequence comparison of DCN1Ls and overall *Gs*-DCN1L structure

(A) A sequence alignment of *G. sulphuraria* (*Gs*), human (*Hs*), and *S. cerevisiae* (*Sc*) DCN1Ls is presented. Secondary structural elements correspond to the *Gs*-Dcn1L structure. Positions of residues involved in cullin-binding as described by Scott et al.[8] are indicated with an asterisk, where red or black indicates interactions that were mediated through main chain or side chain atoms, respectively. The location of Ile244 of *Sc*-Dcn1 is indicated with a dagger. **(B)** The *Gs*-Dcn1L structure is rendered as a cartoon in this stereo pair. α-helices and the N– and C–termini are labeled. For clarity the 9–10 loop is circled and the side chains of residues that are bounded by unmodeled regions of the loop are shown. The protein is colored by B-factor using the visible spectrum, where blue and red indicate relatively low or high B-factors, respectively. **(C)** *Gs*-DCN1L was superposed with the *Sc*-DCN1 of the *Sc*-DCN1/Cdc53 complex (PDB 3O2P). *Gs*-DCN1L is colored as in **(B)**, *Sc*-DCN1 and Cdc53 are colored gray and black, respectively. Selected α-helices and loop-regions are labeled. An asterisk is used to show the position of the disordered *Gs*-DCN1L residues that correspond with the Cdc53 binding region of *Sc*-DCN1

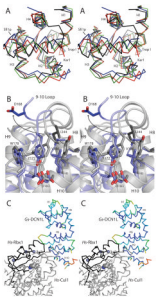

Figure 2. Comparisons of *Gs*-DCN1L with EF-hand containing proteins and *Sc*-DCN1, and modeling of the Cul1-Rbx1-DCN1L complex

(A) The N-terminal EF-hand pair of *Gs*-Dcn1L (black) was superposed with the following EF-hand pair containing proteins: troponin C (green), caltractin (red) and Cdc31p (blue) and rendered as ribbons in this stereodiagram. Helix 5 of *Gs*-Dcn1L and the binding partners of the other EF-hand pairs, Troponin I, Kar1 and Sfi1p, respectively, were not included in the superposition. **(B)** *Gs*-DCN1L (slate) and *Sc*-DCN1 (gray) were superposed and rendered as cartoons in this stereodiagram. Using the *Gs*-DCN1L naming convention, Helices 8–10 were labeled as H8-H10. Residues lining the hydrophobic pocket formed by Helices 8–10 are displayed as sticks. Except for Ile244 of *Sc*-DCN1, all labeled residues correspond to the *Gs*-DCN1L model. The major anchor point of the *Gs*-DCN1L 9–10 loop, Tyr172, is included. A line was drawn between Asp168 of *Gs*-DCN1L and Ile244 of *Sc*-DCN1 to indicate the positional disparity of these sequence related residues, and the gross differences in polypeptide chain morphology between the two respective DCN1Ls. Note that the 9–10 helix of *Gs*-DCN1L was not fully modeled due to its high mobility. **(C)** *Gs*-DCN1L (colored as in Figure 1B) was modeled onto the Cul1-Rbx1 complex (gray and black, respectively), and shown as a stereodiagram. This was accomplished by superposition of *Gs*-DCN1L onto the *Sc*-DCN1/Cdc53 complex (PDB 3O2P), and through superposition of Cdc53 upon Cul1 of the SCF ubiquitin ligase complex (PDB 1LDK). Atoms of the NEDD8 reactive Cul1 residue, Lys720, are shown as spheres.

Table I

Crystal Parameters, Xray Data Collection, and Refinement Statistics

Dataset	Refinement	Peak	Inflection	High remote	Low remote
Crystal parameters[a]					
Unit-cell parameters (Å)	36.7 × 52.4 × 49.1, β=111.2°	36.2 × 51.5 × 48.5, β=110.5°	36.4 × 51.7 × 48.7, β=110.2°	36.4 × 51.6 × 48.7, β=110.3°	36.4 × 51.8 × 48.7, β=110.4°
Data collection statistics[b]					
Wavelength (Å)	0.97625	0.97949	0.97965	0.96427	0.99522
Resolution range (Å)	50.0–1.30 (1.32–1.30)	50.0–1.81 (1.84–1.81)	50.0–1.81 (1.84–1.81)	50.0–1.79 (1.82–1.79)	50.0–1.84 (1.87–1.84)
No. of reflections	42243(1849)	15091(671)	15189(680)	15703(767)	14482(615)
Completeness (%)	98.5(87.2)	97.7(89.7)	97.5(88.1)	98.0(94.5)	97.4(84.2)
R_{merge}[c]	0.040(0.388)	0.075(0.231)	0.074(0.275)	0.074(0.228)	0.076(0.326)
Redundancy	4.0(3.0)	7.5(6.3)	7.5(5.8)	7.5(6.7)	7.4(5.2)
<I>/σ(I)	23.1(2.6)	25.4(10.2)	27.1(8.4)	27.0(11.1)	28.3(5.7)
Refinement and model statistics[b]					
Resolution range (Å)	21.0–1.30 (1.33–1.30)				
No. of reflections (work/test)	40050/2111				
Completeness (%)	98.5(88)				
R_{cryst}[d]	0.156(0.183)				
R_{free}[e]	0.178(0.197)				
RMSD bonds (Å)	0.018				
RMSD angles (°)	1.566				
B factor-overall/ protein/waters ($Å^2$)	20.2/18.6/32.2				
No. of protein molecules/ all atoms[f]	1/1714				
Rama. plot by MOLPROBITY (%)					
Favored region	98.3				
Additionally allowed region	1.7				
Outliers	0				
PDB code	3KEV				

[a] All crystals belonged to the P21 space group.

[b] Values in parentheses are for the highest resolution shell.

[c] $R_{merge}=\Sigma_h\Sigma_i|I_i(h)-\langle I(h)\rangle|/\Sigma_h\Sigma_i I_i(h)$, where $I_i(h)$ is the intensity of an individual measurement of the reflection and $\langle I(h)\rangle$ is the mean intensity of the the reflection.

[d] $R_{cryst}=\Sigma_h||F_{obs}|-|F_{calc}||/\Sigma_h|F_{obs}|$, where F_{obs} and F_{calc} are the observed and calculated structure-factor amplitudes, respectively.

[e] R_{free} was calculated as R_{cryst} using the randomly selected unique reflections (5.01%) that were omitted from structural refinement.

[f] These include atoms from 176 water molecules, acetate ions, and 1 sulfate ion.